TU Delft

Delft University of Technology

Document Version
Final published version

Licence
Dutch Copyright Act (Article 25fa)

Citation (APA)
Pool, D. M., & McKenzie, G. G. (2026). Biodynamic Feedthrough Models and Model-Based Cancellation for Touchscreen Dragging Inputs in Turbulence. In *2025 IEEE Proceedings of the International Conference on Systems, Man, and Cybernetics (SMC) October 5-8, 2025. Vienna, Austria* IEEE.
https://doi.org/10.1109/SMC58881.2025.11343448

Important note
To cite this publication, please use the final published version (if applicable).
Please check the document version above.

Copyright
In case the licence states “Dutch Copyright Act (Article 25fa)”, this publication was made available Green Open Access via the TU Delft Institutional Repository pursuant to Dutch Copyright Act (Article 25fa, the Taverne amendment). This provision does not affect copyright ownership.
Unless copyright is transferred by contract or statute, it remains with the copyright holder.

Sharing and reuse
Other than for strictly personal use, it is not permitted to download, forward or distribute the text or part of it, without the consent of the author(s) and/or copyright holder(s), unless the work is under an open content license such as Creative Commons.

Takedown policy
Please contact us and provide details if you believe this document breaches copyrights.
We will remove access to the work immediately and investigate your claim.

This work is downloaded from Delft University of Technology.

2025 IEEE International Conference on Systems, Man, and Cybernetics (SMC)
October 5-8, 2025. Vienna, Austria

2025 IEEE International Conference on Systems, Man, and Cybernetics (SMC) | 979-8-3315-3358-8/25/$31.00 ©2025 IEEE | DOI: 10.1109/SMC58881.2025.11343448

Biodynamic Feedthrough Models and Model-Based Cancellation for Touchscreen Dragging Inputs in Turbulence

Max McKenzie and Daan M. Pool

***Abstract*— This paper applies model-based biodynamic feedthrough (BDFT) cancellation to a touchscreen dragging task during realistic vertical (vertical) and lateral (horizontal) aircraft turbulence, to mitigate erroneous turbulence-induced inputs. One-size-fits-all (OSFA) BDFT models were used to model the influence of turbulence accelerations on finger position, achieving average quality-of-fits of 61% and 69% in the vertical and horizontal screen directions, respectively. On average, 27% of the touch input error variance was mitigated these OSFA models, with individualized models providing only a marginal improvement (+4%). The application of OSFA models identified from a condition with equally-scaled vertical and horizontal motion (adjusted intensity) to the realistic turbulence condition did not significantly affect cancellation performance, indicating that BDFT models may not need to be adaptive to varying motion intensity. However, consistent with earlier work, BDFT dynamics were found to vary between vertical and horizontal finger movements, with BDFT dynamics exhibiting lower stiffness and a higher static gain for vertical BDFT. On average, the linear BDFT-related component of touch input errors contributed 41% of the overall error variance, indicating that current linear BDFT model may need to be extended to include nonlinear effects, such as varying finger friction.**

I. Introduction

Due to their versatility and efficient use of space, touchscreens are widely used in a variety of applications, ranging from handheld smartphones to electronic flight bags in flight decks [1]. However, using touch interfaces in a vibrating environment has been proven to cause task errors, fatigue, and increased workload [2], [3]. Since in moving vehicles, limbs are inherently perturbed by accelerations, this challenges the implementation of touchscreens in vehicles [4]–[6].

If modelled accurately, the effect of these limb perturbations – known as *biodynamic feedthrough* (BDFT) – can be negated through model-based cancellation [6], [7]. This technology could thereby reduce the need for supporting the hand ergonomically, which is the prevailing mitigation method on flight decks [8], [9]. Model-based cancellation inherently offers more freedom, since users can directly manipulate the display without an intermediary cursor.

The first model-based analysis of BDFT during touchscreen operation was performed by Mobertz et al. [10], who used a multi-sine disturbance perturbation to separate BDFT effects from the inherent stochastic component of human input behavior. A linear mass-spring-damper model was proposed to capture BDFT dynamics, paving the way for the BDFT component of touch input to be removed through model-based cancellation. Multiple experiments [7], [11] have since been performed to investigate the feasibility of model-based BDFT cancellation using the disturbance signals from [10]. Although these previous efforts to model BDFT were successful, no experiment has so far been performed to identify BDFT dynamics with multi-sine disturbances that explicitly match realistic turbulence *and* induce BDFT in both touchscreen input directions simultaneously.

This paper details the results of a human-in-the-loop experiment during which participants were instructed to perform a touchscreen dragging task, whilst perturbed by motion disturbances vertically and horizontally. Seven participants were subjected to disturbance signals that accurately replicate the acceleration experienced during aircraft turbulence. In addition to realistic motion, where the vertical motion intensity is larger than the horizontal, an 'equally scaled' variant of the disturbances was also tested. For the latter case, the signals were scaled so that the motion disturbance in each direction was equally intense.

Control & Simulation, TU Delft Aerospace Engineering, The Netherlands. Email: {g.g.mckenzie, d.m.pool}@tudelft.nl

II. Methodology

This section briefly reviews previous work on model-based BDFT cancellation and how it pertains to this research. Figure 1 shows the underlying mechanisms during the use of a touchscreen under the influence of a motion perturbation. A disturbance signal $f_{d_{y,z}}$ results in involuntary BDFT excitation, indicated with $u_{f_{d_{y,z}}}$, the component of finger movement which is solely due to the disturbance signal. Simultaneously, the user attempts to track a target depending

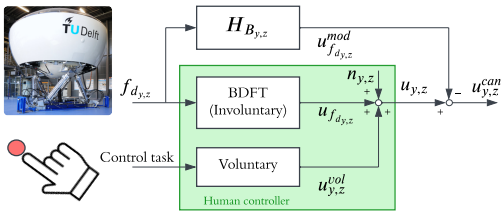


Fig. 1: Schematic overview of BDFT cancellation [7].

on the control task, resulting in a voluntary finger movement component, $u^{vol}_{y,z}$. The final finger position $u_{y,z}$ is then the sum of involuntary and voluntary inputs, next to a remnant $n_{y,z}$ that includes any remaining movement that cannot be attributed to the control task or BDFT. With a model for the BDFT, this involuntary component can be predicted as $u^{mod}_{f_{d_{y,z}}}$ by passing the disturbance through $H_{B_{y,z}}$. Model-based cancellation is achieved by subtracting this estimate from the final input, $u_{y,z}$, resulting in a corrected input, $u^{can}_{y,z}$.

Authorized licensed use limited to: TU Delft Library. Downloaded on March 02,2026 at 12:59:52 UTC from IEEE Xplore. Restrictions apply.

The underlying principle behind BDFT modelling is separation of signal components in the frequency domain, which is possible only by ensuring that $f_{d_{y,z}}$ contains power at a discrete set of frequencies, e.g., a multi-sine [12], [13]. If the disturbance signal were to carry power at all frequencies, as is the case with most realistic signals, then it would not be possible to extract the involuntary component $u_{f_{d_{y,z}}}$ and distinguish it from the remnant.

In this paper, BDFT is modelled using a linear mass-spring-damper and a pure time delay, see (1), where G_B is the static gain, ω_B is the natural frequency, and ζ_B is the damping ratio [10]. A pure time delay τ_B is included to account for hardware latencies in touch input data [14].

$$H_{B_{y,z}}(j\omega) = \frac{G_{B_{y,z}}\omega^2_{B_{y,z}}}{(j\omega)^2 + 2\zeta_{B_{y,z}}\omega_{B_{y,z}}j\omega + \omega^2_{B_{y,z}}} e^{\ \tau_{B_{y,z}}j\omega} \tag{1}$$

Two types of models are used: 1) one-size-fits-all (OSFA), and 2) individualized per participant (IP). OSFA models use parameters that are averaged across all participants for a given condition. Once an OSFA model has been generated, it provides the benefit of not having to identify individuals' BDFT dynamics, instead providing a ready-made solution.

III. Simulator Experiment

A. Experiment Design and Procedures

A human-in-the-loop experiment was performed in the SIMONA Research Simulator at the faculty of Aerospace Engineering at TU Delft, shown in Figure 2b. Three female and four male TU Delft students were recruited, aged 24-30 years. The experiment was approved by TU Delft's Human Resource Ethics Commission (application number 4673) and all participants provided written informed consent.

Participants were seated in the right-hand seat in the simulator cockpit and used the vertically mounted primary flight display (PFD), situated directly in front of them beneath the glare-shield, for touch input. Headsets were used to prevent participants from hearing the motion system's actuators. Participants were instructed to follow a target marker on the screen with the index finger of their preferred hand.

In terms of resistance against BDFT, participants were told to use the target as a general reference and to refrain from exerting any unrealistic, excessive effort to compensate when their finger is inevitably perturbed. Instead of prioritizing performance (minimal tracking error), participants were told to follow the target in a way that could be sustained comfortably across time. This instruction was meant to both prevent fatigue and excessive neuromuscular stiffness in participants, as this could result in unrealistic behaviour.

B. Motion and Target Conditions

During the measurements runs, participants were perturbed by multi-signals in the vertical (Z) and horizontal (Y) directions that accurately represent realistic aircraft motion, obtained from simulating a Cessna Citation II business jet (TU Delft's laboratory aircraft) flying through a Dryden turbulence field [11]. The vertical and lateral accelerations



(a) SIMONA (b) Right-hand seat

Fig. 2: Experiment setup.

are calculated at the pilot's seat, located 3.2 m in front of and 0.75 m above the aircraft's center of gravity. Multi-sines were generated by dividing the measured acceleration spectra into bins, and allocating the summed power of each bin to prime multiples of the base frequency [15], as shown in Figure 3. Between the vertical and horizontal disturbances, 26 distinct frequencies were evenly distributed across the full spectral range (13 sines per direction). This separation of vertical and horizontal frequency components allows for the study of potential cross-coupling effects between directions, i.e., the feeding through of accelerations in orthogonal directions.

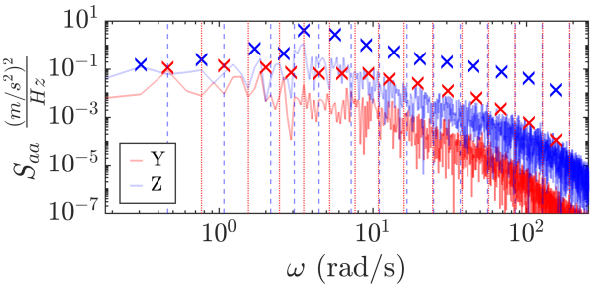


Fig. 3: Multi-sine perturbation signal spectra.

Two scaled variants of the disturbance signals were used during the experiment. The first is the 'realistic' turbulence corresponding to Figure 3, where the final multi-sine signals were scaled for a combined total intensity of 0.75 m/s^2 that retains the realistic relative intensity of the vertical and horizontal accelerations (Z: 0.73 m/s^2, Y: 0.18 m/s^2). The second set of multi-sines were identical, except for a re-scaling so that they had an 'equal' contribution to the total root mean square (RMS) of 0.75 m/s^2, i.e., a vertical/horizontal RMS of $0.75/\sqrt{2} = 0.53$ m/s^2.

For both the 'realistic' (R) and 'equal' (E) disturbance signals, three conditions were tested: 1) only vertical turbulence, 2) only horizontal turbulence, and 3) both horizontal and vertical turbulence. Next to these six conditions, a no-motion (NM) condition was performed for reference, see Table I.

TABLE I: Overview of experiment conditions.

Type	**Realistic (R)**			**Equal (E)**			**NM**
Condition	Y	Z	Z+Y	Y	Z	Z+Y	-
RMS$_y$ (m/s^2)	0.18	0	0.18	0.53	0	0.53	0
RMS$_z$ (m/s^2)	0	0.73	0.73	0	0.53	0.53	0

Authorized licensed use limited to: TU Delft Library. Downloaded on March 02,2026 at 12:59:52 UTC from IEEE Xplore. Restrictions apply.

Each condition consists of three runs with a duration of 45 seconds each, the first of which is discarded in the final analysis to eliminate any training and transient effects as participants adjust to the new condition. The last 40.96 s of each run are used as measurement data, the first 4.04 s are discarded as run-in time. The measurement time corresponds to a base frequency of $\omega_b = 2\pi/40.96 = 0.1534$ rad/s.

To ensure relatively constant finger velocity (and hence a constant screen latency [14]), a circular target marker movement is used with an amplitude of $A_t = 36.2166$ mm at a rate of $\omega_t = 9 \cdot \omega_b = 1.3806$ rad/s. This results in an estimated constant finger speed of $v = \omega_t \cdot A_t = 50$ mm/s, representative for realistic touchscreen operation.

IV. Results

A. Touchscreen Input Error

Figure 4 shows the RMS of the error between the target and finger touch location per condition and direction, revealing that participants' performance was most affected by the Z+Y(E) turbulence on average. For this condition the mean RMS error in horizontal screen direction (red) was 10.22 mm, whereas in the vertical direction (blue) it was 7.48 mm. Given that the turbulence intensity was equal in both directions for this condition, this finding suggests that people are more susceptible to BDFT in the horizontal direction than in the vertical. This is consistent with the Y(E) and Z(E) conditions, which also revealed a difference in horizontal RMS error between 9.29 mm and 6.59 mm, respectively.

For the realistic conditions, participants' performance was most affected during Z+Y(R), achieving average RMS errors of 6.72 mm and 7.90 mm in horizontal and vertical directions, respectively. The superposition of motion in multiple directions seems to have little effect on the error within the realistic conditions (see horizontal lines). Similarly, within the equal conditions, superimposing both directions resulted in only a marginal increase of the mean RMS error for both directions. Two-way Friedman tests revealed that for both types (E/R) and directions (Y/Z), subjecting participants to 2D motion instead of 1D had no significant effect on the error RMS (Z: $\chi^2 = 0.52$, $p = 0.47$, Y: $\chi^2 = 0.29$, $p = 0.59$).

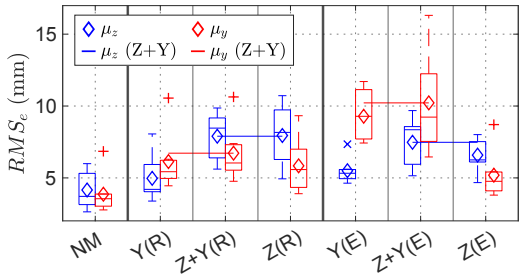
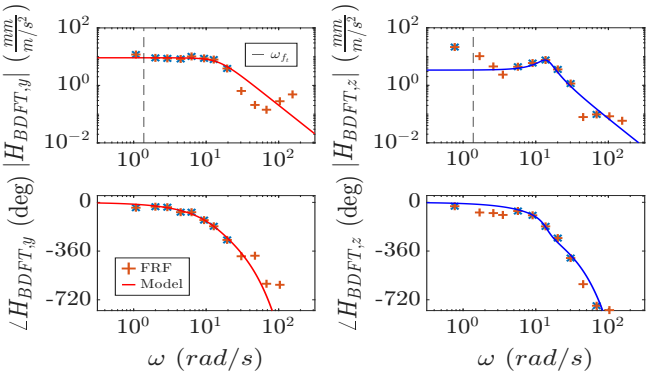


Fig. 4: Root-mean-square of the finger input error.

B. BDFT Frequency Response

Figure 5 shows example BDFT models fitted for participant 5 for the Z+Y(E) motion condition. These models were fitted in the time-domain [16] to optimize the parameters in (1). Frequency components were only included for model identification if the magnitude of the corresponding power spectral density is greater than 3 times that of the local noise level. This heuristically tuned threshold avoids fitting the model to noisy data, but is not overly restrictive. The points that satisfy this requirement are indicated by a blue cross in addition to a plus.

Although the models in Figure 5 are derived from only a single participant's data, certain phenomena can be identified that highlight some of the aggregate results that will follow. For example, comparing Figure 5a and 5b shows that for this participant clearly different BDFT dynamics were observed for the horizontal and vertical directions. Particularly, a higher static gain occurs for horizontal BDFT due to the Y disturbance than for vertical BDFT due to Z turbulence, see the models' y-axis intercept values in Figure 5.



(a) Horizontal (b) Vertical

Fig. 5: BDFT model Bode plots for participant 5, Equal Z+Y; blue crosses indicate $S_{f_d f_d}(j\omega_d)/S_{nn}(j\omega_d) > 3$.

This difference implies increased BDFT susceptibility to horizontal than to vertical disturbances, which may be attributed to two factors. Firstly, in the vertical direction, a person's torso is supported (and constrained) by the seat. This means that the arm tends to pivot around the shoulder, whereas in the horizontal direction, there is no support for the torso except for the sideways friction of the seat. The result is that when subjected to horizontal acceleration, participants' shoulders tend to sway either left or right, since they are essentially pivoting around the base of the seat.

Secondly, from a specific force point of view, simply stretching your arm to the screen already requires compensating for a static 1g downward component. This requires a certain latent neuromuscular activation, regardless of any motion perturbations in the vertical axis. However, in the horizontal direction, the only specific forces are due to the motion perturbation, requiring no latent neuromuscular activation. This asymmetry may cause a difference in admittance and a reduced static BDFT gain in Z compared to Y.

Neuromuscular co-contraction effectively increases the identified stiffness of the BDFT dynamics, and is also known to increase the risk of instability when external perturbations

Authorized licensed use limited to: TU Delft Library. Downloaded on March 02,2026 at 12:59:52 UTC from IEEE Xplore. Restrictions apply.

have power around 2-3 Hz [17]. This is consistent with Figure 5b, where a resonance peak occurs between 10-20 rad/s, due to internal (muscle spindles and Golgi tendon organs) feedback loops. Due to the lower required level of neuromuscular activation, there is less risk of instability (and therefore resonance) in the horizontal direction.

The three lowest frequency FRF points in Figure 5b are seen to deviate from the model, being higher in magnitude. This phenomenon was observed for five out of seven participants during the Z+Y(E) turbulence, but only in Z. As is evidenced by the vicinity around the target frequency (indicated by the dashed line), it is still possible for participants to exert voluntary control at these frequencies. Therefore, participants may apply a deliberate feedback control strategy in an attempt to actively counter the BDFT at low frequencies.

Since such active strategies are not accounted for by the BDFT model of (1), this has a negative influence on its quality-of-fit in terms of variance accounted for (VAF), as calculated by (2). Whereas the VAF for the model fit in Figure 5a amounted to 90.99%, a VAF of only 44.77% was achieved for the vertical BDFT, see Figure 5b. The variance of the first three disturbance frequency components in the measured touch signal amounted to 5.46 mm^2, whereas the variance of the linear component, u_{fd_z}, totalled 9.43 mm^2. As 58% of the linear touch signal variance can be attributed to these first three FRF points, a significantly lower VAF is expected when they are not accounted for by the model.

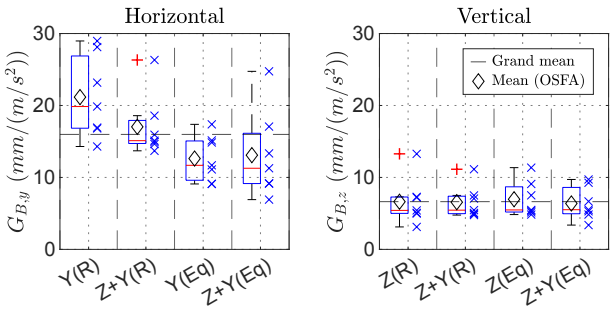
$$\mathrm{VAF}_{z,y} = \left(1 - \frac{\mathrm{var}(u_{fd_{z,y}} - u^{mod}_{fd_{z,y}})}{\mathrm{var}(u_{fd_{z,y}})}\right) \cdot 100\% \qquad (2)$$

C. BDFT Model Parameters

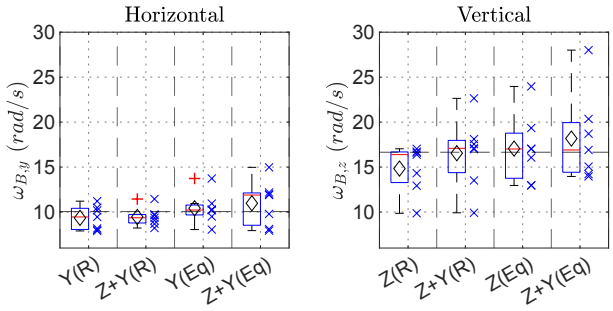
Figure 6a shows the identified BDFT gain for all individualized models, indicating that participants are more susceptible to BDFT in the horizontal direction, as previously noted from Figure 5. The grand mean identified BDFT gain across all participants (dashed horizontal line) was $G_{B,y} = 15.98$ mm/(m/s^2) in Y, and $G_{B,z} = 6.63$ mm/(m/s^2) in Z. Furthermore, the condition with the lowest motion intensity, Y(R), results in the highest identified gains. In the vertical direction, all conditions resulted in approximately the same static gains, indicating a constant level of neuromuscular co-contraction between conditions per direction.

The identified BDFT natural frequency is shown in Figure 6b, showing that the screen input direction is the primary influence on this parameter. Since the natural frequency is a measure of the stiffness-to-mass ratio, and the neuromuscular stiffness is inherently higher in Z than Y, these results are as expected. The mean identified grand means were $\omega_{B,y} = 10.05$ rad/s and $\omega_{B,z} = 16.65$ rad/s for vertical and horizontal screen inputs, respectively.

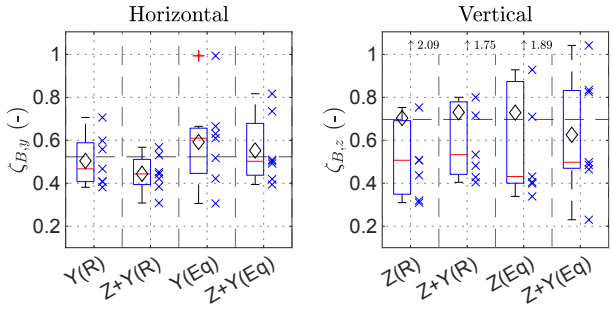
Figure 6c shows the identified damping ratios, which are not significantly affected by direction or condition. More spread and outliers indicating overdamped BDFT dynamics are observed for the vertical direction. These overdamped outliers indicate that a different BDFT model structure may be more suitable, as $\zeta > 1$ indicates fundamentally different dynamics (two real poles) than accounted for in (1).



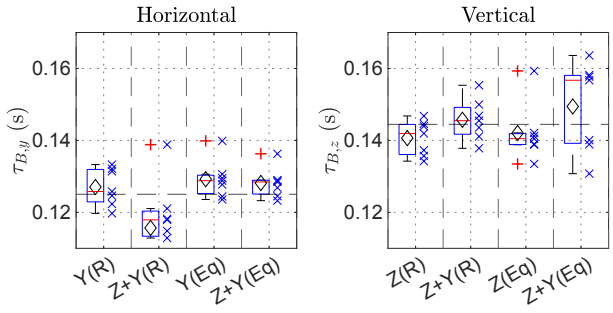
(a) Gain



(b) Natural frequency



(c) Damping ratio

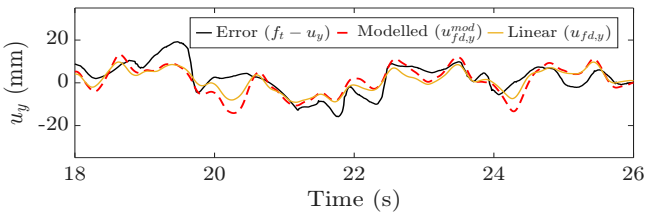


(d) Time delay

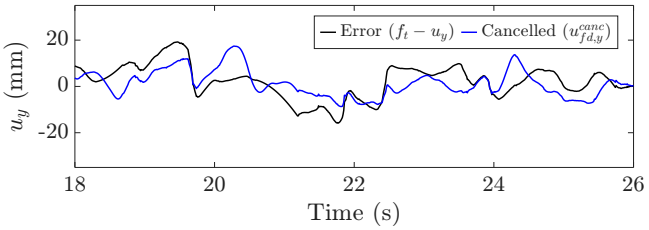
Fig. 6: Individualized (IP) model parameter distributions and corresponding one-size-fits-all (OSFA) values.

Figure 6d shows the identified BDFT time delays, indicating that the vertical direction results in slightly higher time delays than the horizontal direction. The grand means were $\tau_{B,y} = 0.125$ s and $\tau_{B,z} = 0.145$ s, respectively. This could potentially be due to an asymmetry in touchscreen latency between vertical and horizontal screen inputs, which has not yet been explored for the present setup [14].

Authorized licensed use limited to: TU Delft Library. Downloaded on March 02,2026 at 12:59:52 UTC from IEEE Xplore. Restrictions apply.



(a) Identification



(b) Cancellation

Fig. 7: BDFT signal components illustrating model identification (a) and cancellation (b); participant 5, Z+Y Equal.

D. BDFT Cancellation

Figure 7 shows the signal components that are used for BDFT cancellation in time. In this case the total variance of the touch input error equalled $\sigma_e^2 = 54.32$ mm^2. A one-size-fits-all (OSFA) model was used to cancel this BDFT, using model parameters that were averaged across participants for each condition. Although this achieved a VAF of 72.44%, because the variance of u_{fd} is only 25.42 mm^2 (47% of the total variance of the signal), this limits the maximum cancellation that can be achieved, as only the linear component of u is modelled. After cancellation, the variance of the error was reduced by 18.41 mm, (34%). Figure 7 shows that even though the model accurately captures the measured $u_{fd,y}$ (top graph), the final cancelled signal shows that not all erroneous inputs are removed (bottom graph), as $u_{fd,y}^{mod}$ only accounts for less than half of the true input error variance.

This observation from the example BDFT cancellation result in Figure 7 was found to generalize across all participants, conditions, and input directions. This is shown in Figure 8, which also demonstrates how VAF alone is not sufficient to quantify the potency of model-based BDFT cancellation. It is important to also consider the degree to which u_{fd} contributes to the overall variance of the error. For participant 1, an above-average BDFT model VAF was obtained (see dashed line), yes only 48% of the overall error was mitigated after cancellation. Since the variance of the error during no-motion (NM) can either be attributed to target tracking or the remnant, BDFT cancellation can never be expected to eliminate this component of the signal.

On average, 47% of the error signal variance for horizontal inputs can be attributed to BDFT. After cancellation with OSFA models, the total variance is reduced by 25%. For vertical inputs, similar ratios are found, with $u_{fd,z}$ contributing to 50% of the total variance, and BDFT cancellation resulting in a 29% reduction through OSFA models. However, note that more BDFT occurs for lateral than for vertical inputs, with the average total variance being 52.83 mm^2 higher for 'equal' turbulence. Individualized models (data not shown) only result in a marginal 3% and 4% increase in cancelled variance for horizontal and vertical inputs, respectively.

Note that cross-feedthrough from the orthogonal motion direction (yellow bar contributions Figure 8) only accounts for a 7% of the error variance on average. Furthermore, for most cases, the non-BDFT contributions to the error variance ($n_{y,z}$ and $f_{t_{y,z}}$) exceed the no-motion reference (blue lines). This indicates the presence of nonlinearities that are not modelled with the method outlined in section II. The main contributing factor is hypothesized to be frictional contact effects between finger and screen, which are expected to be more prevalent in the presence of motion perturbations.

E. Model Evaluation and Cross-Validation

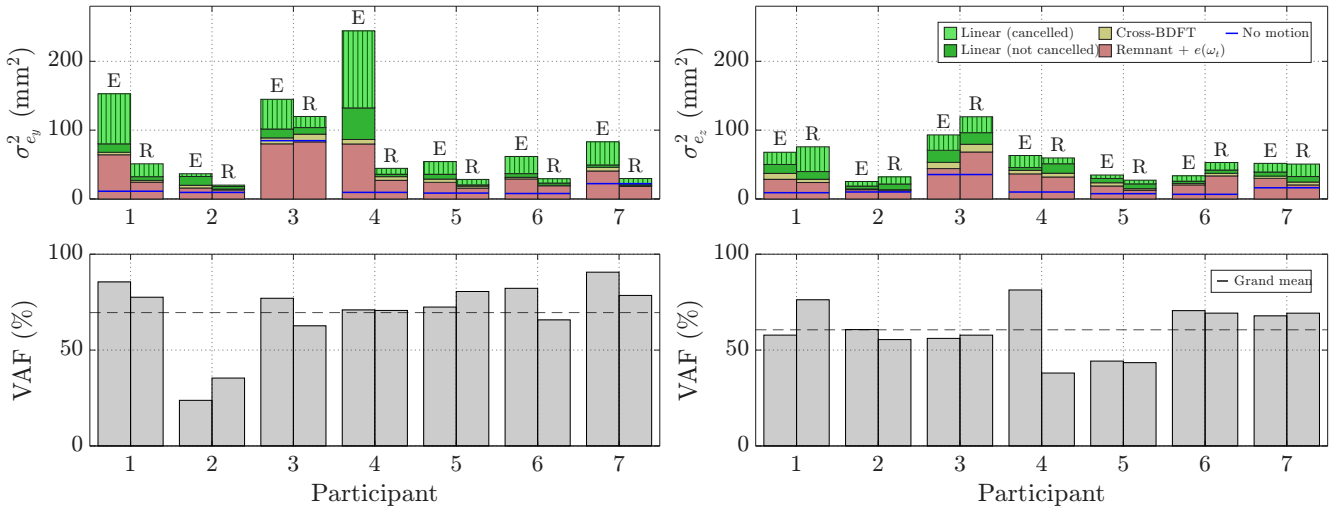
Figure 9 compares the cancellation performance obtained with OSFA models and individualized BDFT models for all conditions. Additionally, the OSFA models identified from the equal (E) conditions were applied to the realistic (R) data to evaluate cross-compatibility (OSFA-CV in black).

A Friedman's test showed that for Z+Y(R), the type of model (IP, OSFA, OSFA-CV) did not have a significant effect on the RMS of u_{fd}^{can} in either screen input direction ($\chi^2 = 6$, $p < 0.05$, for both). This finding suggests that OSFA BDFT models are adequate for cancellation, and that the tested variation in turbulence intensity does not induce changes in BDFT dynamics, e.g., through adapted co-contraction. Finally, even though Figure 8 shows clear differences in BDFT between participants, Figure 9 indicates that OSFA models can still consistently attenuate u_{fd}. In the case of this study, individualized BDFT models resulted in a limited improvement over OSFA models for BDFT cancellation. It is yet uncertain if this result also applies to larger populations, as well as other motion conditions or screen orientations.

V. Conclusion

This paper applied model-based BDFT cancellation to a touchscreen dragging task with (concurrent) vertical and horizontal aircraft turbulence accelerations. The results show that it is feasible to identify and model BDFT dynamics in two touchscreen input directions simultaneously without significantly altering BDFT dynamics compared to when motion disturbances are applied in a single direction only. Furthermore, cross-axis BDFT was found to be negligible, accounting for only 7% of the error variance on average. One-size-fits-all models identified with equally-scaled motion disturbances could be used effectively for cancellation in realistic turbulence conditions, despite different vertical/horizontal acceleration intensities. However, BDFT dynamics were found to clearly differ between screen input directions, with markedly lower stiffness and higher static gains in horizontal (lateral) BDFT than for vertical BDFT. In most cases, over 50% of the variance of the touch input was found to be nonlinear, meaning that despite achieving

Authorized licensed use limited to: TU Delft Library. Downloaded on March 02,2026 at 12:59:52 UTC from IEEE Xplore. Restrictions apply.



(a) Horizontal (b) Vertical

Fig. 8: Variance of horizontal (a) and vertical (b) signal components (top) and corresponding OSFA BDFT model VAF (bottom) for the Equal (E) and Realistic (R) Z+Y conditions per participant.

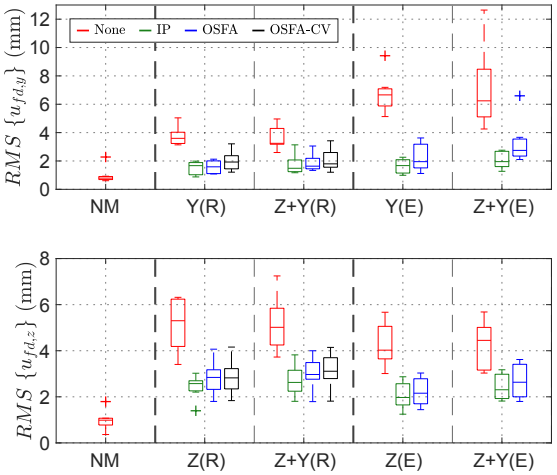


Fig. 9: BDFT cancellation for individual (IP), one-size-fits-all (OSFA), and cross-validation (OSFA-CV) BDFT models.

quality-of-fits of beyond 70%, linear models are fundamentally limited by the linearity of the occurring BDFT. Future work should therefore focus on including nonlinear effects, such as friction and fingertip pressure.

Acknowledgment

This paper is part of the project with number 20624 of the Open Technology Program, financed by the Netherlands Organization for Scientific Research (NWO).

References

[1] H. Avsar, J. E. Fischer, and T. Rodden, "Designing touch-enabled electronic flight bags in sar helicopter operations," in *International Conference on Human-Computer Interaction in Aerospace*, 2016.

[2] A. Cockburn, C. Gutwin, P. Palanque, Y. Deleris, C. Trask, A. Coveney, M. Yung, and K. MacLean, "Turbulent touch: Touchscreen input for cockpit flight displays," in *CHI Conference on Human Factors in Computing Systems*, 2017, p. 6742–6753.

[3] S. Dodd, J. Lancaster, S. Grothe, B. DeMers, B. Rogers, and A. Miranda, "Touch on the flight deck: The impact of display location, size, touch technology & turbulence on pilot performance," 2014.

[4] A. Cockburn, D. Masson, C. Gutwin, P. Palanque, A. Goguey, M. Yung, C. Gris, and C. Trask, "Design and evaluation of braced touch for touchscreen input stabilisation," *International Journal of Human-Computer Studies*, vol. 122, pp. 21–37, 2019.

[5] H. Avsar, J. Fischer, and T. Rodden, "Future flight decks: Impact of +Gz on touchscreen usability," *International Conference on Human-Computer Interaction in Aerospace*, 2016.

[6] D. M. Pool and Y. Vardar, "Fits: Ensuring safe and effective touchscreen use in moving vehicles," *IFAC-PapersOnLine*, vol. 58, no. 30, pp. 248–253, 2024.

[7] A. Khoshnewiszadeh and D. M. Pool, "Mitigation of biodynamic feedthrough for touchscreens on the flight deck," *International Journal of Human–Computer Interaction*, vol. 37, no. 7, pp. 680–692, 2021.

[8] C. B. Watkins, C. Nilson, S. Taylor, K. B. Medin, I. Kuljanin, and H. B. Nguyen, "Development of touchscreen displays for the gulfstream g500 and g600 symmetry™ flight deck," in *2018 IEEE/AIAA 37th Digital Avionics*, 2018, pp. 1–10.

[9] P. R. Thomas, "Performance, characteristics, and error rates of cursor control devices for aircraft cockpit interaction," *International Journal of Human-Computer Studies*, vol. 109, pp. 41–53, 2018.

[10] X. Mobertz, D. M. Pool, M. van Paassen, and M. Mulder, "A cybernetic analysis of biodynamic effects in touchscreen operation in turbulence," *AIAA Modeling and Simulation Technologies Conf.*, 2018.

[11] G. Leto and D. M. Pool, "Effects of turbulence intensity and variability on biodynamic feedthrough modeling in touchscreen dragging tasks," in *AIAA SCITECH 2025 Forum*, 2025.

[12] D. McRuer and H. Jex, "A review of quasi-linear pilot models," *IEEE Trans. on Human Factors in Electronics*, vol. HFE-8, no. 3, 1967.

[13] D. Evans, D. Rees, and D. Jones, "Design of test signals for identification of linear systems with nonlinear distortions," *IEEE Trans. on Instrumentation and Measurement*, vol. 41, no. 6, pp. 768–774, 1992.

[14] S. Vrouwenvelder, F. Postema, and D. M. Pool, "Measuring the drag latency of touchscreen displays for human-in-the-loop simulator experiments," in *AIAA Scitech 2021 Forum*, 2021, pp. 11–15.

[15] M. J. Kolff, K. van der El, D. M. Pool, M. M. van Paassen, and M. Mulder, "Approximating road geometry with multisine signals for driver identification," *IFAC-PapersOnLine*, vol. 52, no. 19, 2019.

[16] P. Zaal, D. Pool, Q. Chu, M. M. Van Paassen, M. Mulder, and J. Mulder, "Modeling human multimodal perception and control using genetic maximum likelihood estimation," *Journal of Guidance Control and Dynamics*, vol. 32, pp. 1089–1099, 2009.

[17] F. van der Helm, A. Schouten, E. Vlugt, and G. Brouwn, "Identification of intrinsic and reflexive components of human arm dynamics during postural control," *J. of neuroscience methods*, vol. 119, pp. 1–14, 2002.

Authorized licensed use limited to: TU Delft Library. Downloaded on March 02,2026 at 12:59:52 UTC from IEEE Xplore. Restrictions apply.